SUBSTRATE DEPENDANCE, TEMPERATURE DEPENDANCE AND TEMPERATURE SENSITIVITY AND RESOLUTION OF DOPED-SILICON MICROCANTILEVERS

BY

ELISE ANNE CORBIN

THESIS

Submitted in partial fulfillment of the requirements
for the degree of Master of Science in Mechanical Engineering
in the Graduate College of the
University of Illinois at Urbana-Champaign, 2009

Urbana, Illinois

Adviser:

Assistant Professor William P. King

Abstract

This thesis aims to characterize microcantilevers with integrated heater-thermometers. This research concentrates on characterization for use in data storage, sensing, surface science, and nano-manufacturing. The first objective seeks to understand the specific thermal interactions between a heated microcantilever tip and various substrates. The experiments investigate thermal conductance, thermal time constant, and temperature-dependant adhesion force between and cantilever tip and substrates of silicon, quartz, and polyimide. The second objective is to utilize a heated microcantilever as a heater-thermometer. The experiments investigate the thermal calibration sensitivity and resolution under steady and periodic conditions near room-temperature. The results were compared to the Raman spectroscopy, which measures the local temperature at the cantilever tip.

to my family,

with love

Acknowledgments

I appreciate the many people who supported me during my time at the University of Illinois. Many thanks to my adviser, Dr. William P. King, who saw my enthusiasm and willingness to work and invested in me. I also want to thank all of my group members for their guidance and special thanks to Dr. Jungchul Lee, Dr. Keunhan Park, and Dr. Zhenting Dai for their guidance, and help to make some sense of the confusion through my research. I am grateful to all my friends for their support and contributions to my work.

Finally, thanks to my family for their eternal love and support. Thanks for being there even on the late teary nights when I was losing faith in myself. And for enduring through this process with me, giving me confidence, and never losing faith in me.

Table of Contents

List of Tables

List of Figures

Chapter 1

Introduction

1.1 Atomic Force Microscopy

Atomic Force Microscopy (AFM) has become one of the most widely used tools for sensing and actuating on the nanometer scale [1]. An AFM uses a microcantilever with a sharp tip in order to obtain a topography. A vertical piezoelectric actuator under the substrate maintains either constant contact force between the cantilever and the substrate (contact mode) or oscillating amplitude of the cantilever force (tapping mode) using an appropriate feedback mechanism. As the tip is raster-scanned across the surface, it is deflected as it moves over the surface contours and optical sensing is used to track the deflection. The optical sensor employs a laser that is reflected from the back of the reflective AFM cantilever and onto a position-sensitive detector (photodiodes).

1.2 Heated Microcantilevers

Advances to this field have lead to the development of the heated microcantilever which was originally designed for thermomechanical data storage [2, 3], but its capabilities have since been expanded to include nanoscale thermal instrumentation, nanomanufacturing, nanometrology, nanotopography [4, 5, 6], thermal reading and writing. A heated microcantilever that was fabricated from doped single crystal silicon is shown in figure 1.1. Electrical current in the cantilever induces resistive heating at the cantilever free end. The fabrication and characterization of these cantilevers is well understood, and are discussed below.

1.2.1 Design and Fabrication

The heated microcantilevers were made using a standard silicon-on-insulator (SOI) process [7], and their fabrication is briefly stated as follows. The cantilevers are made from an SOI wafer of orientation $\langle 100 \rangle$, and n-type doping at 2×10^{14} cm^{-3} having a resistivity of approximately 4 Ω-cm. The cantilever tip was

formed using an oxidation sharpening process [8], and has a height between 500 nm and 1 μm, with a tip radius of and had a radius of a curvature near 20 nm. The cantilever was doped using two phosphorous steps: first, the two parallel cantilever legs were doped to 1×10^{20} cm^{-3} and then the heater region near the free end of the cantielver was doped to 1×10^{17} cm^{-3}. The doping makes the heater region of size of 8×16 μm^2 more resistive than the rest of the cantilever.

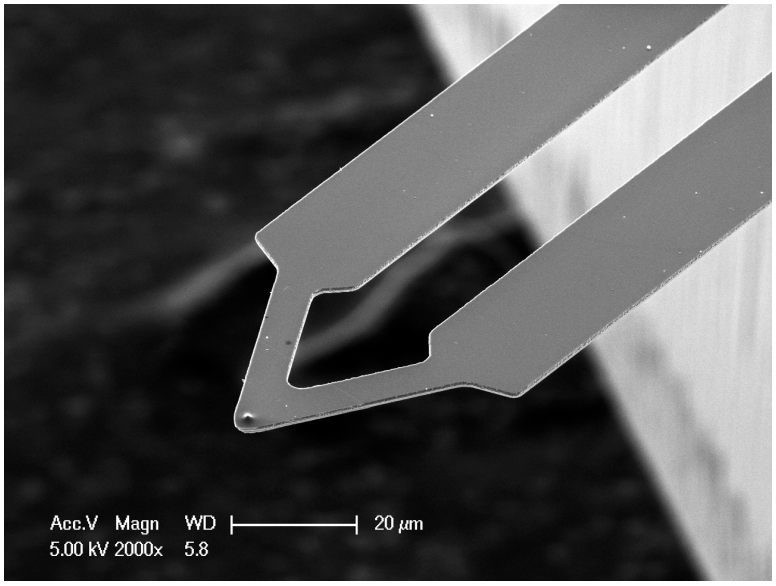

Figure 1.1: Scanning Electron Microscopy image of a Heated Microcantilever

In this "U-Shaped" configuration, when an electrical current is applied through the cantilever the cantilever tip will heat up. More than 90% of the power is dissipated in the highly resistive heater region, resulting in a temperature increase that can exceed 1300 K [9]. Figure 1.2 shows an infrared image of the heated microcantilever, which verifies that heating occurs only near the free end of the cantilever [9].

1.2.2 Device Characterization

The electrical characterization of the heated microcantilever is well understood [9] and was conducted using a simple "sense" circuit, shown in Figure 1.3. The cantilever was mounted in the circuit, where it was connected in series to a resistor in order to protect it by limiting the current at high power as well as to measure the current during excitation. A resistor with a high resistance of 10kΩ was used. Figure 1.4 depicts the DC response of a cantilever with a 10kΩ resistor in air, without interacting with a substrate, and it can be seen that the electrical resistivity response of the cantilever is nonlinear. The resistance of the cantilever increases as the applied voltage increases because of the decreasing electrical mobility of doped silicon with temperature. As the DC response of the cantilever peaks around 600°C it begins to

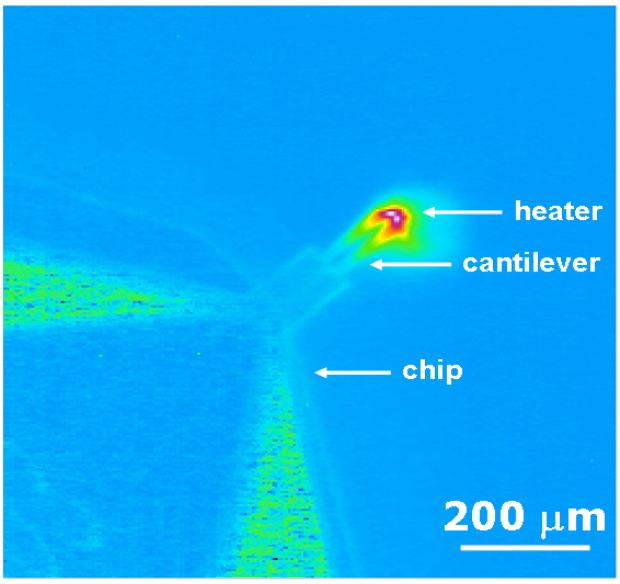

Figure 1.2: Infrared image of a heated microcantilever confirming heating at the tip

decrease, which is called "thermal runaway" due to the thermally generated intrinsic carriers outnumbering the doped carriers [7].

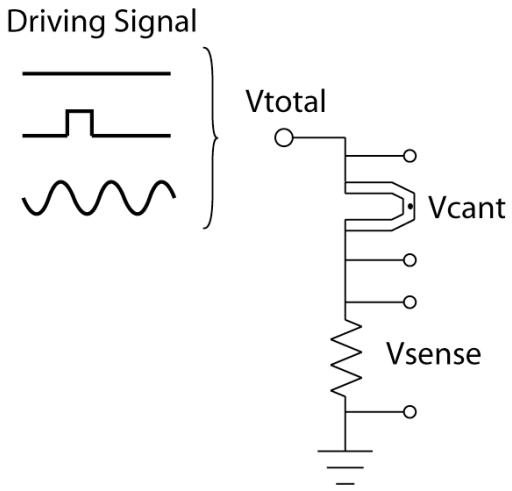

Figure 1.3: "Sense" circuit used to characterize the cantilever. There is a sense resistor connected to the cantilever in series to protect the cantilever at high power and to sense the current during excitation.

Temperature around the cantilever tip, collected using Raman spectroscopy, is shown in figure 1.5. Raman scattering has been used to determine temperature distribution with micron spatial resolution in silicon [10, 11, 12]. Overall, the cantilever can reach temperatures $> 600\,^{\circ}\mathrm{C}$ and the cantilever resistance is a strong function of temperature. In order to accurately measure the temperature rise in the cantilever many aspects of the Raman optical scattering signature must be utilized. The position of the Stokes peak,

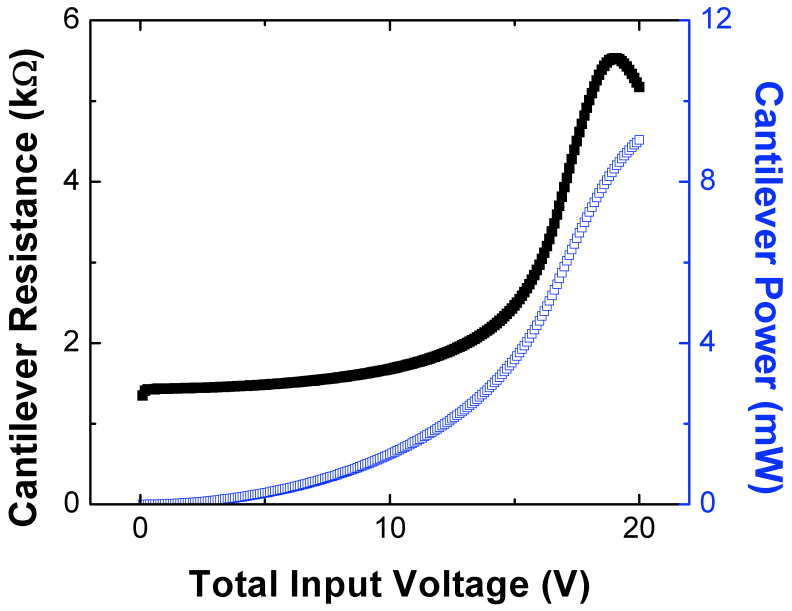

Figure 1.4: Cantilever DC response of cantilever resistance vs input voltage and power vs input voltage

the width of the Stokes peak, and the ratio of the Stokes peak to the anti-Stokes peak are all methods for determining the temperature. The first of these methods is the least accurate due to the fact that the Stokes peak contains both stress data and temperature data; however, the other two methods require extremely long accumulation times. Because the stresses are small upon the cantilever we can measure the Stokes peak quickly and accurately to get a good value for the temperature by assuming that the stresses are negligible.

The interaction between the cantilever and the substrate requires precise mechanical properties of the cantilever such as the spring constant and resonance frequency. A thermal noise calibration technique is the method used in the commercial AFM system (MFP-3D, Asylum research) to address these calibration issues. The spring constant is given by $k = \frac{k_B T}{\langle x^2 \rangle}$, where k is the cantilever spring constant, k_B is Boltzmann's constant, T is the cantilever temperature, and $\langle x^2 \rangle$ is the mean square deflection of the cantilever, which can be determined from integrating a simple harmonic oscillator model fit of the power spectrum of the cantilever thermal vibrations. At room temperature, the measured resonant frequency was ~ 70 kHz, as shown in the Figure 1.6, and the spring constant was found to be ~ 0.6 N/m. At higher temperature, the spring constants was found decreases specifically at 400 °C to be ~ 0.3 N/m. The interaction between the cantilever and substrate, and how it is affected by cantilever properties, is discussed in further detail in Chapter 2.

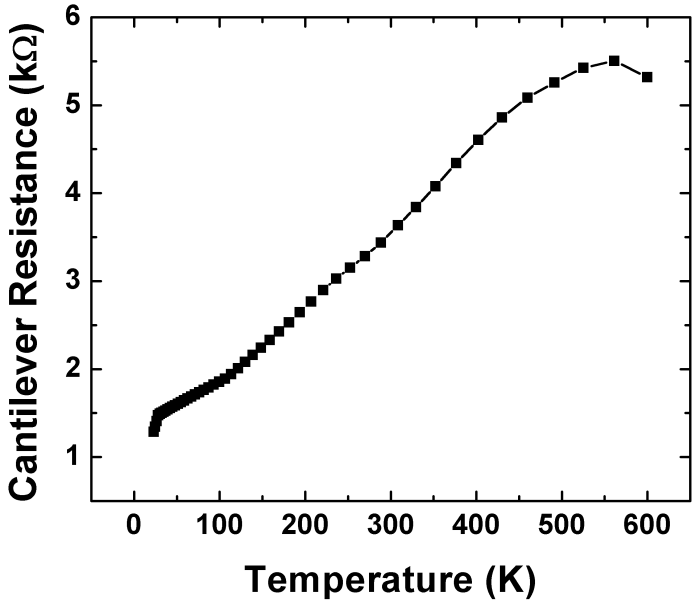

Figure 1.5: Cantilever DC response of cantilever resistance vs. temperature

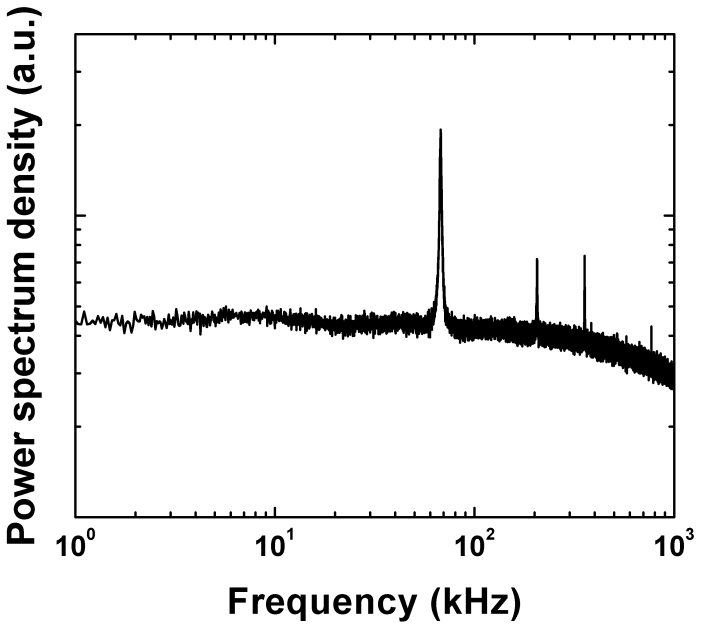

Figure 1.6: The mechanical characteristics of the cantilever when it is suspended in quiescent air, without interacting with the substrate. The noise density spectrum of the cantilever provides the fundamental mechanical resonance frequency of the cantilever.

1.3 Objectives

Chapter 2 investigates the specific thermal interactions between a heated microcantilever tip and various substrates. The utilization of heated microcantilevers for surface science, nano-manufacturing, data storage, and sensing were widely investigated and require improved understanding of their fundamental thermal and mechanical behavior while interacting with different substrates. The heat flow from a thermal microcantilever changes with respect to different surfaces and their individual properties, which must be adequately characterized. These results aid new applications of heated cantilevers in surface analysis and metrology that may allow for the recognition of polymorphic changes upon undetermined substrates.

Chapter 3 describes how an atomic force microscope microcantilever, having an integrated solid-state resistor, can be used as a heater or a resistive thermometer. The thermal calibration sensitivity and resolution of these cantilevers was investigated under steady and periodic operation near room-temperature. Overall, the temperature coefficient of resistance of the cantilever is 0.0029 K^{-1} near 300 K. When the cantilever is placed under periodic heating conditions the temperature resolution is measured as low as 5 mK. This characterization of heated cantilevers enables precise measurement of small temperature changes, and could improve nanoscale thermal measurements.

Chapter 2

Substrate Dependance of Thermal Conductance, Time Constant, and Temperature-Dependant Adhesion of Heated Microcantilevers

2.1 Introduction

Microcantilever heaters, AFM cantilevers having integrated solid-state heating elements, have been widely investigated for uses in data storage, sensing, surface science, and nano-manufacturing [3, 13]. These applications require improved understanding of the fundamental thermal and mechanical behavior of heated microcantilevers while interacting with different substrates. Cantilever thermal and mechanical characterization in air [9] as well as heat flow between a microcantilever tip and a semiconductor surface have been closely examined [14]. However, much less work has been done to understand the specific thermal interactions between a heated microcantilever tip and different substrates, even though relevant substrates can have physical properties spanning several orders of magnitude. This chapter reports measurements of substrate thermal conductance, thermal time constant, and temperature-dependant adhesion force between and cantilever tip and substrates of silicon, quartz, and polyimide (with the aim of creating new opportunities for the use of heated AFM cantilevers).

The experiments were performed using heated AFM microcantilevers, which have an integrated resistor heater at the free end and are described in more detail in Chapter 1. A simple sense circuit, which is shown figure 1.3, is used to operate and characterize the microcantilever and is explained in more detail in the previous chapter. A general DC analysis in quiescent air at 25 °C was performed, and the results are displayed in figure 1.3 which shows the nonlinearity of the cantilever resistance with respect to the total input voltage. As an applied electrical current flows through the microcantilever it induces resistive heating at the free end which is measured using Raman spectroscopy (described in more detail in the previous chapter) and the cantilever resistance as a function of the cantilever heater temperature is shown in figure 1.4.

2.2 Experiments

2.2.1 Force versus Distance Curves

One technique for analyzing substrate properties (i.e. elasticity) is force versus distance curves, which are used to measure the tip-substrate interaction force that the cantilever tip applies to the surface. A force vs. distance curve is actually a plot of the deflection of the cantilever, which has been converted based on the spring constant of the cantilever against the extension of the z-direction piezo. Therefore, it can be clearly seen how the cantilever approaches, contacts, and the retracts from the surface. These different steps can be seen in figure 2.1 which shows a schematic of how the force of the cantilever tip applied to the surface varies with distance.

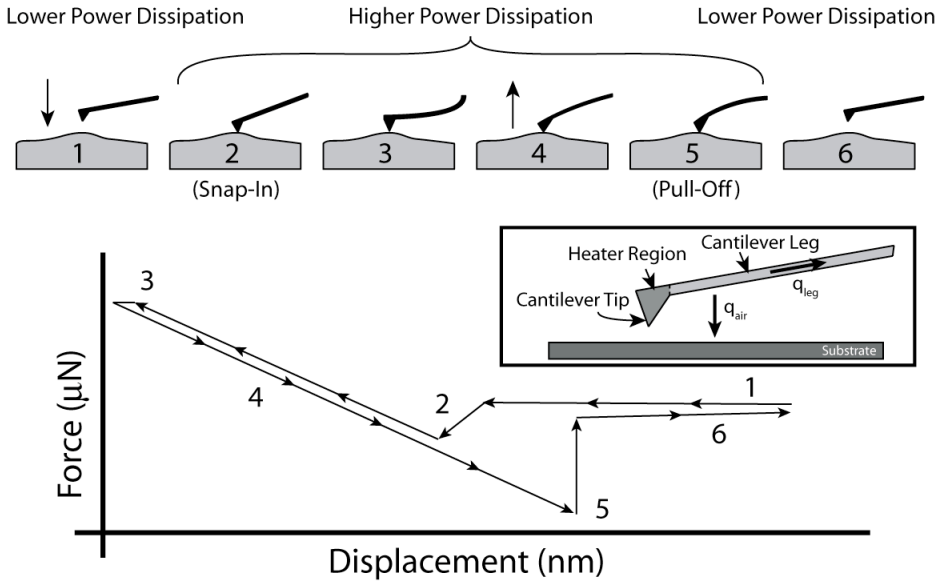

Figure 2.1: As the probe approaches a substrate the dissipated heat from the cantilever will increase, while maintaining a constant temperature (thermal resistance). The fluctuation in power across the cantilever is the obtained thermal signal.

In brief, the principles of the force-distance measurements involve the probe approaching the substrate, which may cause the probe to bend upwards due to repulsive forces (step 1), until it jumps into contact with the surface, or "snaps-in," by local Coulombic forces (step 2). Then the force is increased in the contact region, which in turn increases the cantilever deflection (step 3). The probe begins retraction (step 4) until the tip is freed from the surface (step 5) and then returns to the equilibrium position (step 6). The force-distance curve often shows a hysteresis, seen in step 5, referred to as the "pull-off" force, which can be used to estimate the surface energy or the binding forces.

2.2.2 Tip-Substrate Thermal Conductance

Thermal microcantilevers measure the heat dissipated on a surface in response to resistive heating by an applied voltage. Using this, in combination with knowledge about heat transfer, we are able to infer information about the topography as well as some surface properties of a material that is brought into close proximity to the microcantilever. Heat flow from a cantilever is a strong function of the air gap, therefore changes in position can be measured through the changes in thermal resistance caused by the heaters integrated into the cantilevers. The inset of figure 2.1 describes how a microcantilever senses a surface. As the probe approaches a substrate the air gap closes and the thermal resistance will decrease, causing the cantilever temperature to vary while maintaining a constant heating power. As the probe then moves away from a substrate, the thermal resistance between the cantilever and the substrate increases, again causing a change in the cantilever temperature. The thermal signal acquired from the microcantilever can then be used to produce a thermal image and perform other thermal analyses. Using the measurement of the force vs. distance curve the thermal conductance between the cantilever and substrate can be investigated as a function of cantilever-substrate distance.

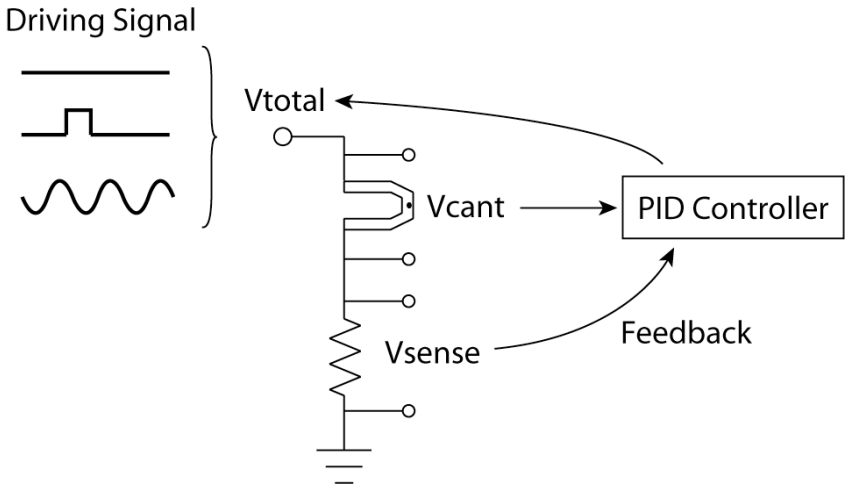

Figure 2.2: This is the sense circuit used with a PID control in order to maintain a constant resistance to watch the power fluctuate. There is a sense resistor connected to the cantilever in series to protect the cantilever at high power and to sense the current during pulse excitation. A high-speed amplifier is configured when the cantilever is operated with a sense resistor having high resistance.

Experimental setup used is the same "sense" circuit, but with a proportional-integral-derivative (PID) controller. A PID controller is a generic control loop feedback mechanism used to correct the error of a desired setpoint by calculating and then outputting a corrective action that can adjust the process accordingly and rapidly, to keep the error minimal. As described above, the cantilever approaches and retracts from contact with the substrate causing both the cantilever resistance and dissipated power to

fluctuate. To remove one variable from the system the PID controller was used to maintain the resistance of the cantilever in order to ensure that the power is the only fluctuating value in the system, shown in figure 2.2. Force vs. distance data was acquired simultaneously with the thermal signal from the cantilever. Knowing that only the power was dissipated, the thermal conductance, G, can be calculated from the power dissipated, q, and the change in cantilever temperature, ΔT, by dividing cantilever heating power by the temperature difference between cantilever temperature and room temperature ($q/\Delta T$).

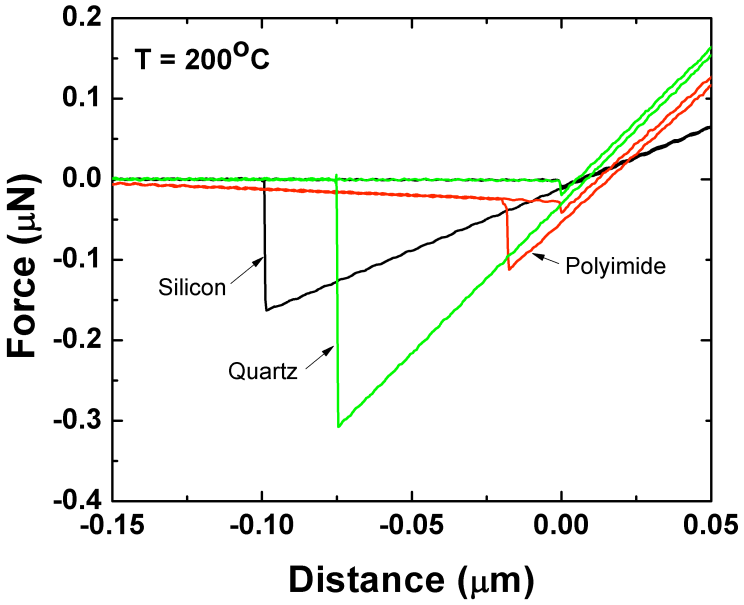

Figure 2.3: Force vs. distance curve for silicon, quartz, and polyimide at 200 °C.

Conductance measurements were made over a range of temperatures on three surfaces: quartz, silicon, and polyimide. Figure 2.4 shows the force and thermal conductance between the heated cantilever and the three different substrates for a cantilever heated to 300 °C. The cantilever speed was 2 microns per second and it dwelled on the surface for 1 second.

There was some slight variation of the conductance to air of the cantilevers, because multiple cantilevers need to be used with slightly different characteristics. It was found that for a cantilever far from a substrate, the measured conductance to air was 0.03419 mW/K, 0.03601 mW/K, and 0.03481 mW/K for the cantilever associated with quartz, silicon, and polyimide substrates, respectively. For the cantilever in contact with each of these substrates at 200 °C, the thermal conductance was found to be 0.03443 mW/K, 0.03624 mW/K, and 0.03497 mW/K, respectively. As temperature increased there was an overall decreasing trend of the thermal conductance for all of the materials, which is to be expected for

these materials.

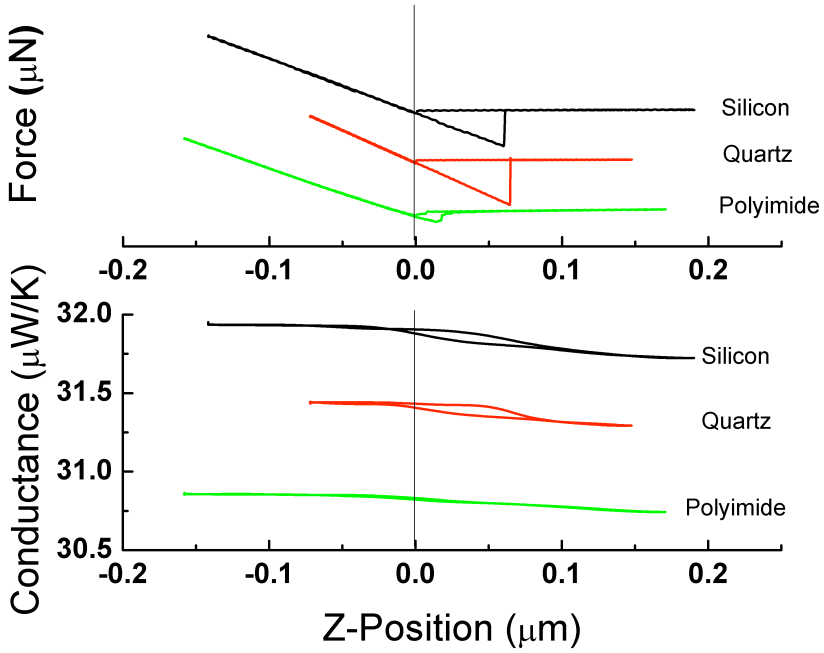

Figure 2.4: Cantilever force and cantilever conductance vs. tip-substrate distance (Z-Position) for several substrates. These experiments were repeated across all surfaces for varying cantilever temperatures and on surface dwell times.

2.2.3 Pull-Off Force and Work Adhesion

From a force vs. distance curve there are two distinguishable regions to be noted. First of which is during the approach, where as the cantilever gets close to the surface the tip will be first repulsed by the surface then attracted to the surface by van der Waals forces. It is at this point of attraction that the van der Waals forces will take over and the cantilever will "snap in" to the surface, or basically the point at which the cantilever is now considered in contact with the surface, which can be seen in figure 2.1. The force required to break tip-substrate contact is the "pull-off" force, shown in figure 2.1. Secondly, as the cantilever retracts from the surface an adhesion force dominates the cantilever deflection until the cantilever is released from the surface. The pull-off force, F, was calculated using Hooke's Law by multiplying the maximum cantilever deflection, d, before the tip is pulled off the surface, by the spring constant of the cantilever, k. The work of adhesion is the energy required to overcome adhesion between the tip and the substrate, and can be calculated by integrating the force-distance product during pull-off. Figure 2.5 shows the force vs. distance curves of silicon at a range of temperatures.

The pull-off force and work of adhesion of silicon, polyimide, and quartz substrates were measured

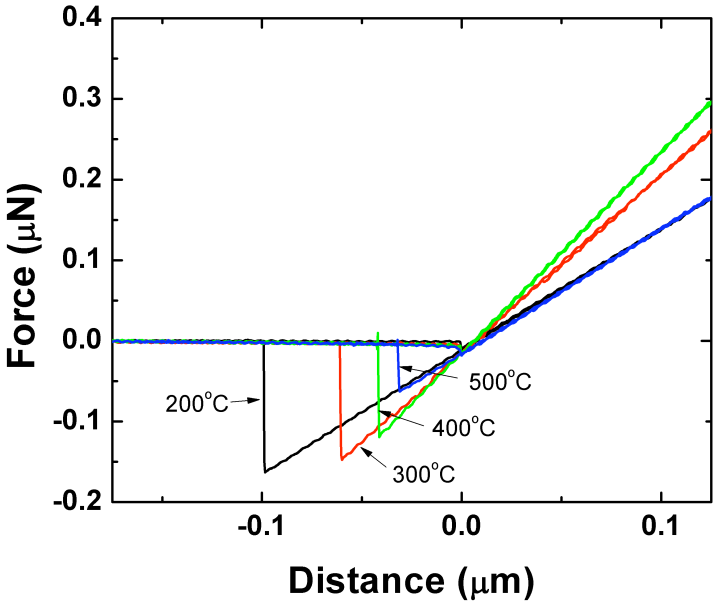

Figure 2.5: Force vs. distance curve of silicon at a range of temperatures. The experiments were repeated with varying dwell times on the surface.

under different temperature conditions as well as varying on surface dwell time. The pull-off force and work of adhesion results are presented in table 2.2.3. Overall, the trends between these two quantities follow the same trends, which makes sense since both the pull-off force as well as the work adhesion are related to the amount of hysteresis in the curve, which would make them proportional. Figure 2.7 and 2.6 show a decreasing trend of energy and pull-off force, respectively, for quartz and silicon with increasing temperature, whereas polyimide showed an increasing trend. At higher temperatures adhesion decreases; however in the case of polyimide the material becomes malleable above its melting temperature allowing for the cantilever to become embedded into the material accounting for the increasing trends. It can be seen from the results that silicon had a higher value for pull-off force than polyimide, but quartz had higher than both of these substrates. These relationships held for work adhesion as well, which is to be expected.

2.2.4 Cooling Time Constant

In order to take thermal measurements accurately with the heated microcantilever, adequate timing for heating and cooling will have to be accounted for. The proper time required to heat and cool the microcantilever is directly related to the underlying physics of the device. The heating time constant of the microcantilever has already been fully investigated, and measurements of cooling cycles were taken to investigate the cooling time constant.

Table 2.1: Pull-Off Force and Work Adhesion Results

Pull-Off Force

Substrate	Temperature (°C)	Dwell 1s	Dwell 2s	Dwell 3s	Dwell 4s	Dwell 10s
Silicon	200	165.35	168.64	163.95	163.27	158.87
Silicon	300	143.19	118.33	115.99	128.65	123.83
Silicon	400	117.15	146.29	138.61	139.12	146.46
Silicon	500	60.737	37.64	31.54	34.50	29.22
Polyimide	200	15.79	15.35	5.35	18.17	33.92
Polyimide	300	17.42	18.53	18.80	14.64	19.43
Polyimide	400	32.47	24.84	42.29	25.35	34.23
Polyimide	500	33.60	8.61	34.78	27.91	30.12
Quartz	200	328.86	360.65	368.08	374.16	390.91
Quartz	300	188.30	210.45	219.33	229.38	235.53
Quartz	400	134.97	130.43	159.35	159.07	162.65
Quartz	500	99.45	97.83	106.46	105.19	103.53

Work of Adhesion

Substrate	Temperature (°C)	Dwell 1s	Dwell 2s	Dwell 3s	Dwell 4s	Dwell 10s
Silicon	200	8.57	8.33	8.10	7.79	7.60
Silicon	300	4.32	3.86	3.74	3.65	3.23
Silicon	400	2.46	3.83	3.41	4.32	4.85
Silicon	500	1.02	0.55	0.29	0.48	0.31
Polyimide	200	1.45	1.29	1.01	1.36	1.33
Polyimide	300	0.69	0.84	0.88	1.02	1.04
Polyimide	400	2.28	1.75	1.68	1.70	1.53
Polyimide	500	3.34	3.81	3.88	3.52	4.62
Quartz	200	13.23	15.78	16.07	17.01	17.58
Quartz	300	6.15	7.69	8.36	8.92	9.44
Quartz	400	4.15	4.71	5.85	5.82	5.90
Quartz	500	2.90	2.82	3.35	3.35	3.17

To calculate the cooling time constant, a square voltage pulse was applied to the cantilever, and the system response was recorded. After the pulse elapsed, the thermal response of the cantilever decayed exponentially to its original temperature. The Agilent 33250A function generator supplied DC and square pulse voltage excitation while the Agilent 34401A digital multimeter and Agilent Infiniium 54831B oscilloscope measured the voltage drop across the sense resistor with DC and pulse excitation, respectively. With this instrumentation, the cantilever electrical resistance and power dissipation was obtained. Square pulses of amplitudes ranging from 1 V to 4 V, and duration times ranging from 1 μs to 30 ms were applied to the cantilever with a 0.5 V DC offset to monitor the resistance before and after the pulse. Figure 2.8 displays an excitation pulse applied to the cantilever along with a generalized response. Experimental data was fit exponentially to determine the cooling time constant, and figure 2.9 summarizes the the

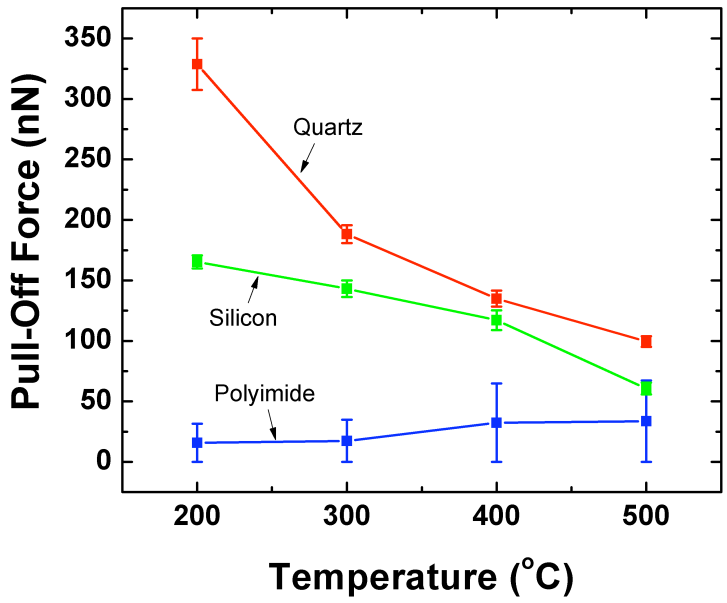

Figure 2.6: Pull off force vs. temperature for several substrates. The experiments were repeated across all surfaces for varying cantilever temperatures and on surface dwell times.

measurement results for all three surfaces: quartz, silicon, and polyimide.

The heated cantilever can cool to room temperature from about 300 °C for a short heating time (1μs) in approximately 50 ns. For long heating times, as fast as 0.1 ms in air as well as 0.1 ms, 0.3 ms, and 0.15 ms for silicon, quartz, and polyimide, respectively. Overall the time constant remained fairly steady for the pulse widths less than 1 ms and amplitude, and appear to plateau after the jump at 1 ms.

2.3 Conclusions

Substrate thermal conductance, thermal time constant, and temperature-dependant adhesion force between and cantilever tip and substrates were measured to enhance the understanding of thermal interactions between a heated microcantilever tip and different substrates. These results aid new applications of heated cantilevers in surface analysis and metrology that may allow for the recognition of polymorphic changes upon undetermined substrates.

It was found that the conductance measurements showed a decreasing trend with an increase in temperature with the cantilever in contact with each of the substrates. The results from the force distance curves for depicting the pull-off force as well as the work adhesion showed some interesting trends as well. For silicon and quartz there is a general decrease in both the "pull-off" force and work adhesion with an

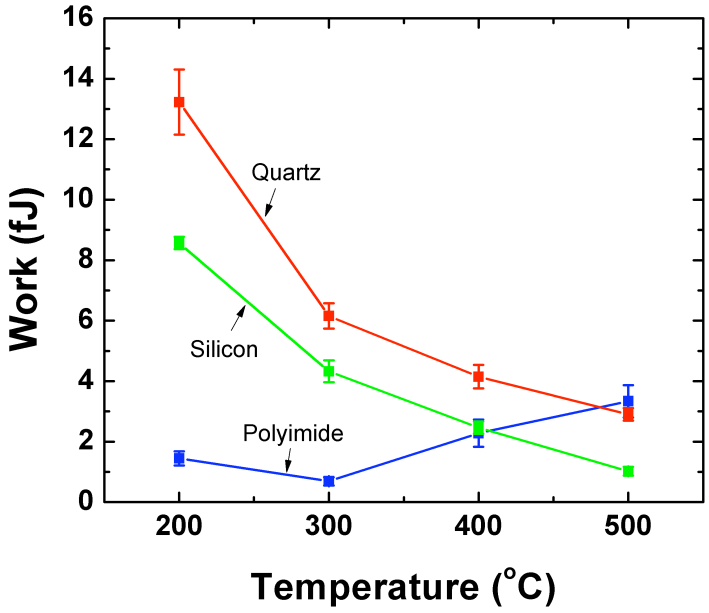

Figure 2.7: Work vs. temperature for several substrates. The experiments were repeated across all surfaces for varying cantilever temperatures and on surface dwell times.

increase in temperature. Whereas, polyimide there is the opposite or reverse effect, due to the malleability of the material as the temperature passes its melting point. These trends are related due to the nature of the hysteresis of the force-distance curve in that as the pull-off force is increased so is the work adhesion. Finally, the cooling time constant at long heating times were 0.1 ms, 0.3 ms, and 0.15 ms with the cantilever tip placed on the silicon, quartz, and polyimide surfaces, which provides information about the possible speed capabilities of these heated cantilevers for thermal reading and writing.

The decreasing trend of the work adhesion and the pull-off force with increasing temperature can be explained due to the increase in energy in the system in order to overcome adhesion. For the polyimide the tip is actually penetrating the surface and therefore lifting out a mass with it which would change the amount of initial deflection accounting for the approach slope that it is seen. Along with the additional mass there will be a change in the tip radius which would increase the adhesion forces, leading to inaccuracies or error in the measurements. Since the polyimide would be partially covering the tip, the tip-surface interaction would change due to the fact that it is now a new material at the tip.

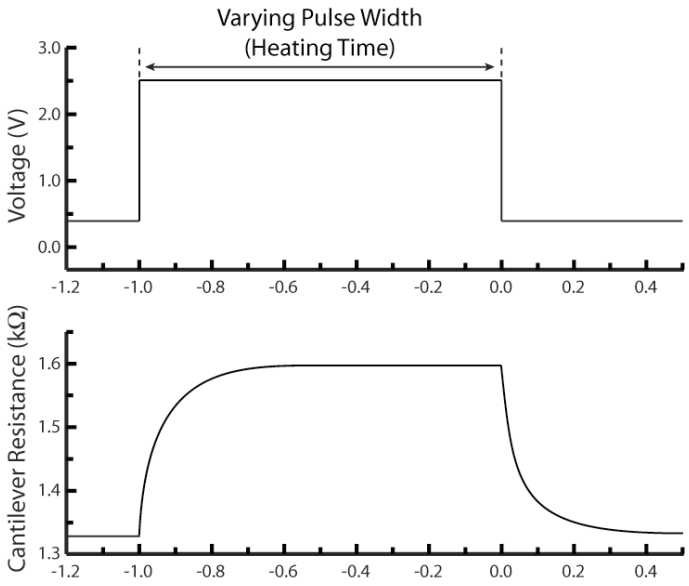

Figure 2.8: Generalized square pulses and the cantilever response of varying amplitudes and varying duration times.

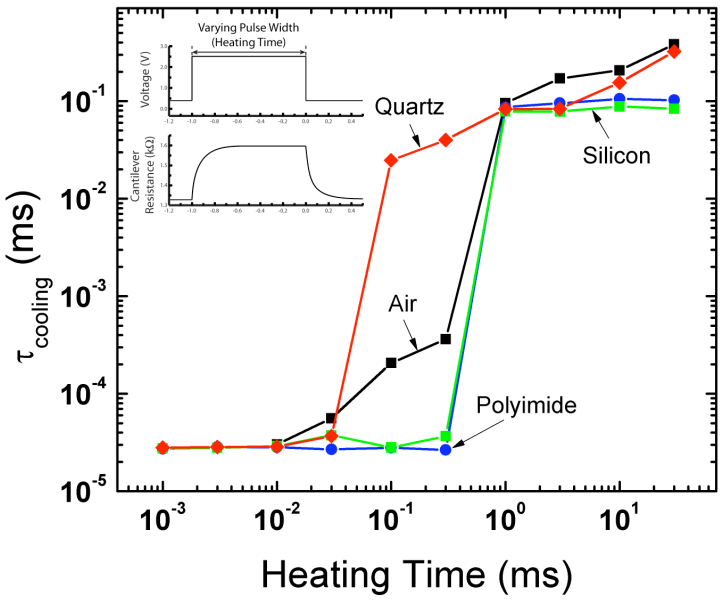

Figure 2.9: Square pulses of amplitudes ranging from 1 V to 4 V, and duration times ranging from 1 μs to 30 ms were applied to the cantilever with a 0.5 V dc offset to monitor the resistance before and after the pulse.

Chapter 3

Room-Temperature Temperature Sensitivity and Resolution of Doped-Silicon Microcantilevers

3.1 Introduction

Recent advances of atomic force microscopy (AFM) have evolved nanoscale thermal instrumentation, such as scanning thermal microscopy (SThM) [15], nano-thermal analysis (n-TA) [16, 17], and near-field photothermal infrared spectroscopy (PTIR) [18, 19]. These techniques are capable of mapping thermal or chemical information with unprecedented spatial resolution. The common key issue in realizing these promising metrologies is the precise measurement of a small temperature rise in a highly localized manner, and has motivated the development of a thermal AFM probe whose tip is functionalized as either a thermocouple [20, 21, 22] or a resistive heater-thermometer [7, 9, 23]. The spatial resolutions achievable with thermal probes have been well investigated, revealing 50 nm for the thermocouple probe [21] and 140 nm for the heater-thermometer probe [14] dominantly due to a sub-100 nm tip radius. The temperature sensitivity near room temperature is very important for many types of measurements, but temperature sensitivity has not been carefully studied below about 50 °C [9, 24]. The temperature resolution is also very important, particularly near room temperature. Therefore the temperature resolution near room temperature of thermal probes was a fully investigated for these emerging applications.

As shown in Figure 3.1, the doped-silicon probe has a low-doped region integrated at the free end that functions as either a heater or a resistive thermometer [9]. This probe has been adopted for various nanoscale thermal applications, including data storage [2], nanolithography [25, 26], self-cleaning spectroscopic nanosampling [27], and electrothermal scanning gate microscopy [28], most of which require the local heating capability above 200 °C. Previous studies have demonstrated that the doped-silicon probe can increase the tip temperature up to 1000 °C, and function reliably in vacuum [29], cryogenic [30], and liquid [31] environments. However, thermal behaviors of the probe near room temperature have not been rigorously characterized. Several applications of thermal probes would benefit from room temperature thermal characterization, especially infrared measurements and photothermal infrared spectroscopy

(PTIR), which require sub-100 mK temperature measurements. The experimental investigation on the room-temperature temperature sensitivity and resolution of the doped-silicon probe will thus facilitate its further use as a sensitive thermometer near room temperature.

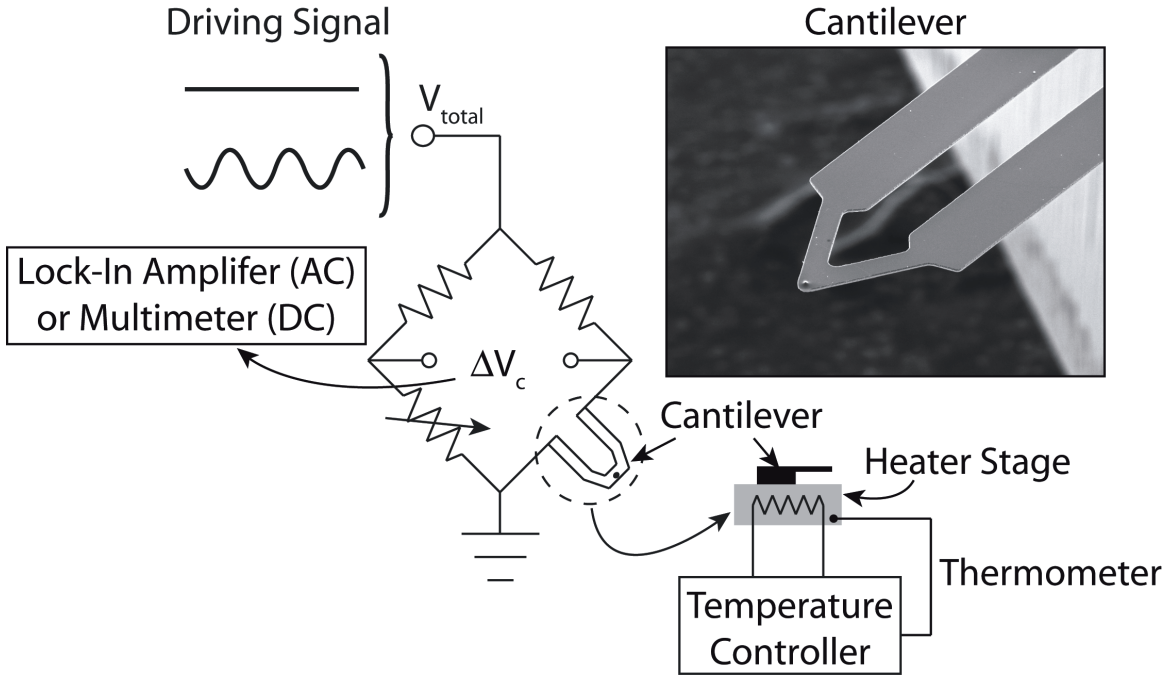

Figure 3.1: An SEM image of the heated microcantilever and the schematic diagram describing the ac and dc characterization experiment. AC characterization is performed with a function generator and lock-in amplifier. DC characterization is performed with a dc power supply and multimeter.

3.2 Experiment

Figure 3.2 shows the experimental setup where the doped-silicon microcantilever was attached to a temperature-controlled heater stage. The experimental setup was insulated to exclude interference from the environment. While the heater stage temperature was closed-loop controlled within a ∼20 mK uncertainty, the cantilever signal was differentially measured in a Wheatstone bridge with 1 kΩ resistors through the potential difference between A and B, i.e., $\Delta V_C = V_B - V_A$. The cantilever can be operated in either steady (DC) mode or periodic (AC) mode when it is to be used as a thermometer. DC characterization is straightforward to measure a steady ΔV_C using a multimeter under a steady input voltage. For the AC characterization, ΔV_C has harmonic signals under a sinusoidal input voltage and thus can be measured with a lock-in amplifier.

As long as the temperature rise is small, the electrical resistance of the cantilever can be linearized as

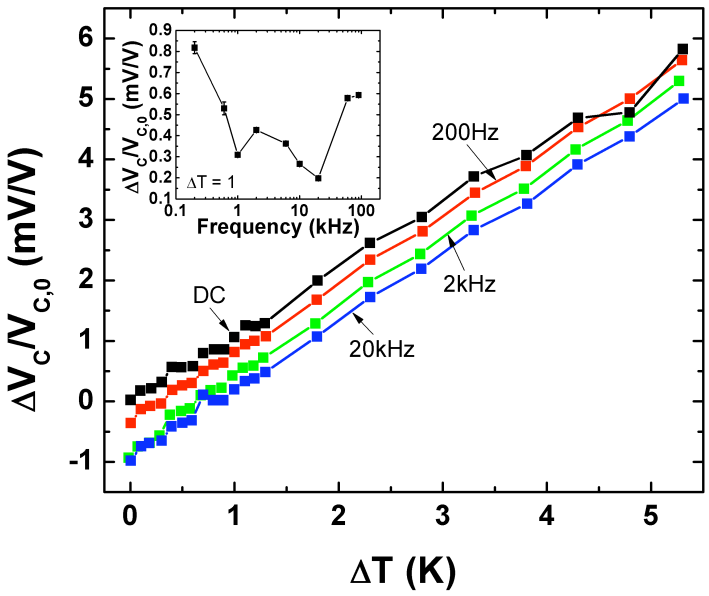

Figure 3.2: The measured results on the electrical and thermal responses of the cantilever. Relative Change in cantilever voltage corresponding to temperature change relative to room temperature. The inset is the normalized drop across the cantilever vs frequency at a maintained ΔT at 1 K.

$R_C = R_0[1 + \alpha\Delta T]$, where R_0 is the cantilever resistance at a reference temperature, α is the temperature coefficient of resistivity (TCR), and ΔT is the temperature rise of the heater stage. In DC mode, if the voltage drop across the potentiometer V_C is set the same as that across the cantilever at the reference temperature, the cantilever voltage change can be approximated as $(\Delta V_C/V_{C,0})_{dc} \approx [R_1/(R_1 + R_0)]\alpha\Delta T$, where is the cantilever voltage at the reference temperature, and the sense resistance of the Wheatstone bridge. Thus the temperature can be monitored in real time simply by measuring the cantilever voltage, while the sensitivity is $S = [R_1/(R_1 + R_0)]\alpha\Delta T$. In order to prevent self-heating, the input voltage V_{total} is maintained at 10 mV, corresponding to the cantilever power dissipation of 24 nW and, equivalently, the cantilever tip temperature increase < 2 mK.

In AC mode, the cantilever voltage has three harmonics due to periodic power dissipation of the cantilever and the resultant cantilever resistance oscillation [32]. The second and third harmonic signals are two orders of magnitude smaller than the first harmonic signal [30, 32] and induce negligible temperature rise. The first harmonic cantilever signal can then be approximated as $(\Delta V_C/V_{C,0})_{ac} \approx (R_1\alpha\Delta T - j\omega R_1 C_C)/(R_1 + R_0 + j\omega R_1 R_0 C_C)$, where C_C is the parasitic cantilever capacitance connected in parallel with the cantilever resistance [30, 33]. The cantilever capacitance is around 10−100 pF depending on the cantilever geometries and operation condition, and its effect on the

cantilever electric behaviors is negligibly small up to 30 kHz [30, 33]. Although not shown here, the out-of-phase cantilever voltage signal, the imaginary part of the above equation, is six orders of magnitude smaller than the in-phase signal even at 100 kHz, consistent with the previous studies. Thus the AC cantilever signal can be further simplified the same as the DC case, i.e., $(\Delta V_C/V_{C,0})_{dc} \approx [R_1/(R_1+R_0)]\alpha\Delta T$, suggesting that the AC cantilever signal be a linear function of the temperature and have the same slope as the DC cantilever signal. However, the noise level will be much lower in AC mode compared to DC mode, resulting in better temperature resolution.

Figure 3.2 shows the cantilever voltage change as a function of the temperature rise ΔT for both steady and periodic signals. Note that for the periodic operations only the in-phase cantilever voltages are plotted in figures, as the out-of-phase cantilever voltage is negligibly small. The slope of the temperature response for the AC signals is similar to that of the DC temperature response, which confirms that the both signals are linear functions of temperature with the same sensitivity. The inset of Figure 3.2 shows a snapshot at $\Delta T = 1$K of the cantilever signal versus the measured frequency range.

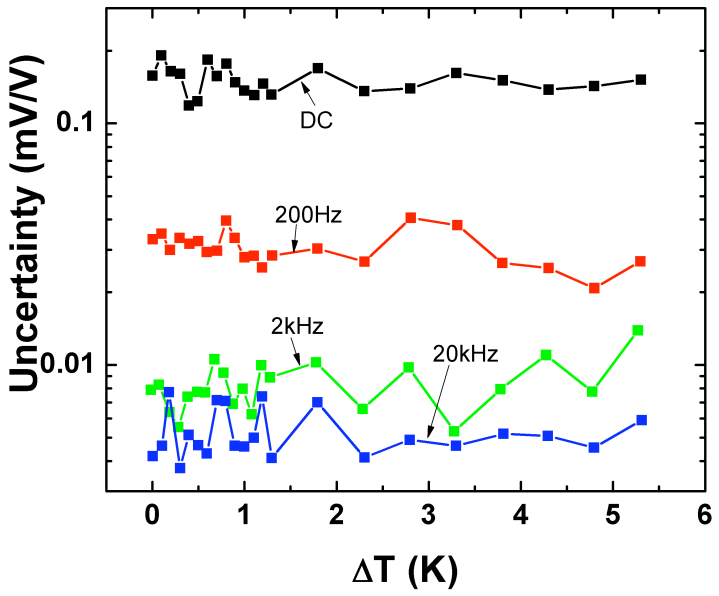

Figure 3.3: Uncertainty of the percent change in cantilever voltage corresponding to temperature change relative to room temperature.

The uncertainty of a signal is critical in determining the measurement resolution for a small temperature change. Figure 3.3 shows the uncertainty of the cantilever signal as a function of temperature rise, ΔT. The uncertainty of the periodic signal is an order of magnitude smaller than that of the steady signal. This is expected since the lock-in amplifier can be relatively insensitive to noise because it is only

retrieving one frequency at a time. The uncertainty was routinely measured without a special care and thus includes all measurement and environment noise sources.

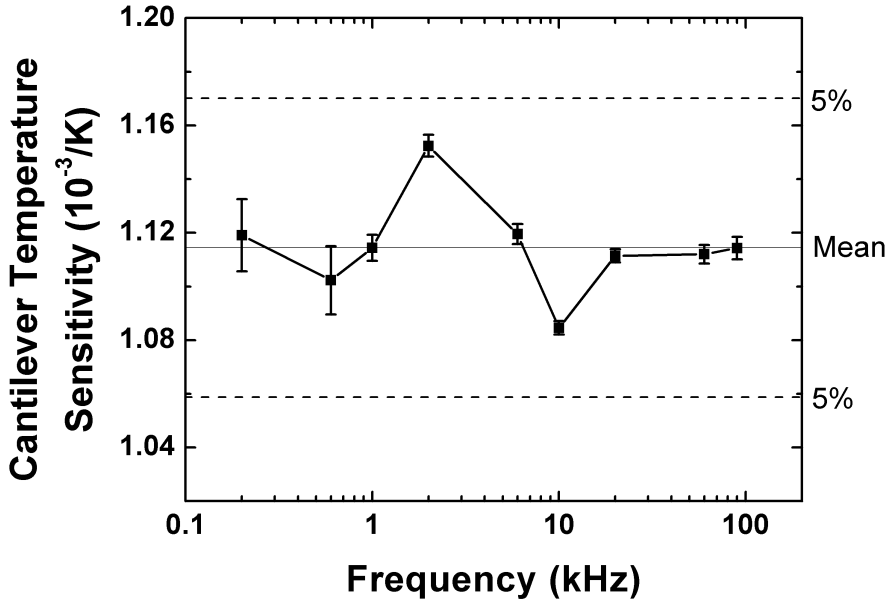

Figure 3.4: Comparison of the cantilever sensitivity vs frequencies with a fixed input voltage at 10mV-rms. Across the frequency range the sensitivity maintains within 5% of its mean value.

The cantilever temperature sensitivity, or TCR, is the cantilever signal per change in temperature, $\Delta V_C/V_C/\Delta T$, or in other words, the slope of the data displayed in Figure 3.2. The cantilever temperature sensitivity (10^{-3}/K) is compared at different frequencies of the AC signal and is shown in Figure 3.4. Across the investigated frequency range the sensitivity has a small fluctuation within 5% of its mean value. The mean sensitivity of the microcantilever is 0.0011 K^{-1}, or equivalently 0.0029 K^{-1} as the mean TCR of the cantilever. This value is around 75% of the TCR of bulk platinum (Pt), 0.0039 K^{-1}, and more than twice as sensitive as previously reported micro/nano-thermometers such as a Pt nanothermometer (0.0007 K^{-1}) [14], an electro-deposited Pt nanowire (0.0014 K^{-1}) [34], and a polycrystalline Pt nanofilm (0.0013 K^{-1}) [35]. The temperature resolution of the cantilever indicates the smallest step change in temperature that could be measured in a given integration time and can be determined by the noise, or average uncertainty U_{avg}, and the sensitivity S, i.e., U_{avg}/S. Figure 3.5 shows the cantilever temperature resolution over a range of frequencies. When compared with the DC temperature resolution over 100 mK, the AC measurement improves the temperature resolution by more than one order of magnitude, achieving the smallest resolution of 5 mK at 10 kHz. For operation frequency over 20 kHz, the temperature resolution begins to increase with a larger uncertainty because the electrical impedance plays a significant

role in the cantilever response [33].

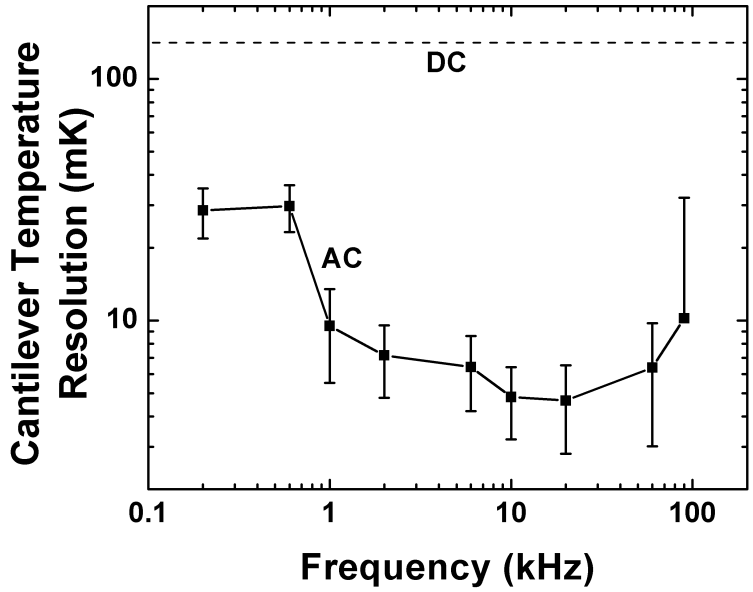

Figure 3.5: The cantilever resolution of temperature over different frequencies. This is found by the average uncertainty divided by the sensitivity

A Raman spectroscope measured cantilever temperature with DC electrical excitation, yielding an uncertainty of ±2.1 K for a temperature range of 300 to 500 K [**?**]. Comparing the above results to the Raman calibration, the cantilever TCR obtained in the present study, 0.0029 K^{-1}, falls within the uncertainty of the TCR determined from the Raman experiment, K^{-1}. Moreover, the impedance of the cantilever can be calculated for the AC operation, and the change of the resistance remains stable with respect to change in temperature. The relative stability of the resistance with respect to change in temperature in combination with the small uncertainty suggests quantitatively that this method for temperature calibration, near room temperature, is far more accurate than Raman spectroscopy.

3.3 Conclusions

This chapter reports the temperature sensitivity and resolution of a doped-silicon microcantilever probe near room temperature. For both steady (DC) and periodic (AC) operation, the cantilever signal has a linear relationship to the change in temperature relative to the room temperature. The temperature resolution for the AC mode is estimated to be as small as 5 mK, more than 20 times smaller than that of the DC mode. This temperature resolution is sufficiently low to measure infrared signals near room

temperature, and will enable sensitive measurements for fundamental heat transfer studies and infrared spectroscopy.

Chapter 4

Summary and Conclusions

In this study, analyses of the substrate dependance of thermal conductance, time constant, and temperature-dependant adhesion of heated microcantilevers, as well as the room-temperature temperature sensitivity and resolution of doped-silicon microcantilevers, was presented in this work. A closer examination of heated microcantilever tips and their fundamental thermal and mechanical behavior while interacting with different substrates for use in surface science, nano-manufacturing, data storage, and sensing was investigated in this thesis. The heat flow from a thermal microcantilever changes with respect to different surfaces and their individual properties, and the characterizations presented previously will allow for improved use of heated microcantilevers with all substrates. These results aid new applications of heated cantilevers in surface analysis and metrology that may allow for the recognition of polymorphic changes upon undetermined substrates.

The conductance measurements showed a decreasing trend with an increase in temperature with the cantilever in contact with the all the substrates. The results from the force distance curves for depicting the pull-off force as well as the work adhesion showed two important trends. For silicon and quartz there is a general decrease in the "pull-off" force and the work adhesion with an increase in temperature. Whereas, polyimide there is the opposite or reverse effect, due to the malleability of the material as the temperature passes its melting temperature. These trends are related due to the nature of the hysteresis of the force-distance curve in that as the pull-off force is increased so is the work adhesion. Also, the heated cantilever can cool to room temperature from about 300 °C for a short heating time (1μs) in approximately 50 ns. And for long heating times, as fast as 0.1 ms in air as well as 0.1 ms, 0.3 ms, and 0.15 ms for silicon, quartz, and polyimide, respectively.

The use of a heated microcantilever as a heater-resistive thermometer was used to investigate the thermal calibration sensitivity and resolution under steady and periodic operation near room-temperature. Overall, the temperature coefficient of resistance of the cantilever is 0.0029 K^{-1} near 300 K. When the cantilever is placed under periodic heating conditions the temperature resolution is measured as low as 5

mK. This characterization of heated cantilevers enables precise measurement of small temperature changes, and could improve nanoscale thermal measurements.

References

[1] Binnig, G., C. Quate, and C. Gerber (1986) "Atomic Force Microscope," *Physical Review Letters*, **56**(9), pp. 930–933.

[2] King, W. P., T. W. Kenny, K. E. Goodson, G. L. W. Cross, M. Despont, U. T. Durig, H. Rothuizen, G. Binnig, and P. Vettiger (2002) "Design of atomic force microscope cantilevers for combined thermomechanical writing and thermal reading in array operation," *Journal of Microelectromechanical Systems*, **11**(6), pp. 765–774.

[3] Vettiger, P., G. Cross, M. Despont, U. Drechsler, U. Durig, B. Gotsmann, W. Haberle, M. Lantz, H. Rothuizen, R. Stutz, and G. Binnig (2002) "The "millipede"- Nanotechnology entering data storage," *IEEE Transactions on Nanotechnology*, **1**(1), pp. 39–55.

[4] King, W., T. Kenny, and K. Goodson (2004) "Comparison of thermal and piezoresistive sensing approaches for atomic force microscopy topography measurements," *Applied Physics Letters*, **85**(11), pp. 2086–2088.

[5] Kim, K. J., K. Park, J. Lee, Z. M. Zhang, and W. P. King (2007) "Nanotopographical imaging using a heated atomic force microscope cantilever probe," *Sensors and Actuators A-Physical*, **136**(1), pp. 95–103.

[6] Park, K., J. Lee, Z. M. Zhang, and W. P. King (2007) "Topography imaging with a heated atomic force microscope cantilever in tapping mode," *Review of Scientific Instruments*, **78**(4), p. 7.

[7] Chui, B. W., T. D. Stowe, Y. S. Ju, K. E. Goodson, T. W. Kenny, H. J. Mamin, B. D. Terris, R. P. Ried, and D. Rugar (1998) "Low-stiffness silicon cantilevers with integrated heaters and piezoresistive sensors for high-density AFM thermomechanical data storage," *Journal of Microelectromechanical Systems*, **7**(1), pp. 69–78.

[8] Ravi, T., R. Marcus, and D. Liu (1991) "Oxidation Sharpening of Silicon Tips," *Journal of Vacuum Science & Technology B*, **9**(6), pp. 2733–2737.

[9] Lee, J., T. Beechem, T. L. Wright, B. A. Nelson, S. Graham, and W. P. King (2006) "Electrical, thermal, and mechanical characterization of silicon microcantilever heaters," *Journal of Microelectromechanical Systems*, **15**(6), pp. 1644–1655.

[10] Viera, G., S. Huet, and L. Boufendi (2001) "Crystal size and temperature measurements in nanostructured silicon using Raman spectroscopy," *Journal of Applied Physics*, **90**(8), pp. 4175–4183.

[11] Ostermeir, R., K. Brunner, G. Abstreiter, and W. Weber (1992) "Temperature Distribution in Si-MOSFET's Studied by Micro Raman-Spectroscopy," *IEEE Transactions of Electron Devices*, **39**(4), pp. 858–863.

[12] Perichon, S., V. Lysenko, B. Remaki, D. Barbier, and B. Champagnon (1999) "Measurement of porous silicon thermal conductivity by micro-Raman scattering," *Journal of Applied Physics*, **86**(8), pp. 4700–4702.

[13] King, W. P., S. Saxena, B. A. Nelson, B. L. Weeks, and R. Pitchimani (2006) "Nanoscale thermal analysis of an energetic material," *Nano Letters*, **6**(9), pp. 2145–2149.

[14] Park, K., G. L. W. Cross, Z. M. M. Zhang, and W. P. King (2008) "Experimental investigation on the heat transfer between a heated microcantilever and a substrate," *Journal of Heat Transfer-Transactions of the Asme*, **130**(10), p. 9.

[15] Majumdar, A. (1999) "Scanning thermal microscopy," *Annual Review of Materials Science*, **29**, pp. 505–585.

[16] Hammiche, A., L. Bozec, M. Conroy, H. M. Pollock, G. Mills, J. M. R. Weaver, D. M. Price, M. Reading, D. J. Hourston, and M. Song (2000) "Highly localized thermal, mechanical, and spectroscopic characterization of polymers using miniaturized thermal probes," *Journal of Vacuum Science & Technology B*, **18**(3), pp. 1322–1332.

[17] Nelson, B. A. and W. P. King (2007) "Measuring material softening with nanoscale spatial resolution using heated silicon probes," *Review of Scientific Instruments*, **78**(2), p. 8.

[18] Reading, M., D. Grandy, A. Hammiche, L. Bozec, and H. M. Pollock (2002) "Thermally assisted nanosampling and analysis using micro-IR spectroscopy and other analytical methods," *Vibrational Spectroscopy*, **29**(1-2), pp. 257–260.

[19] Hammiche, A., L. Bozec, M. J. German, J. M. Chalmers, N. J. Everall, G. Poulter, M. Reading, D. B. Grandy, F. L. Martin, and H. M. Pollock (2004) "Mid-infrared microspectroscopy of difficult samples using near-field photothermal microspectroscopy," *Spectroscopy*, **19**(2), pp. 20–+.

[20] Luo, K., Z. Shi, J. Varesi, and A. Majumdar (1997) "Sensor nanofabrication, performance, and conduction mechanisms in scanning thermal microscopy," *Journal of Vacuum Science & Technology B*, **15**(2), pp. 349–360.

[21] Shi, L., O. Kwon, A. C. Miner, and A. Majumdar (2001) "Design and batch fabrication of probes for sub-100 nm scanning thermal microscopy," *Journal of Microelectromechanical Systems*, **10**(3), pp. 370–378.

[22] Lee, D. W., T. Ono, and M. Esashi (2002) "Fabrication of thermal microprobes with a sub-100 nm metal-to-metal junction," *Nanotechnology*, **13**(1), pp. 29–32.

[23] Dai, Z., W. P. King, and K. Park (2009) "A 100 nanometer scale resistive heater-thermometer on a silicon cantilever," *Nanotechnology*, **20**(9), p. 9.

[24] Nelson, B. A. and W. P. King (2007) "Temperature calibration of heated silicon atomic force microscope cantilevers," *Sensors and Actuators A: Physical*, **140**(1), pp. 51–59.

[25] Nelson, B. A., W. P. King, A. R. Laracuente, P. E. Sheehan, and L. J. Whitman (2006) "Direct deposition of continuous metal nanostructures by thermal dip-pen nanolithography," *Applied Physics Letters*, **88**(3), p. 3, iSI Document Delivery No.: 004MO Times Cited: 24 Cited Reference Count: 26 AMER INST PHYSICS.

[26] Szoszkiewicz, R., T. Okada, S. C. Jones, T. D. Li, W. P. King, S. R. Marder, and E. Riedo (2007) "High-speed, sub-15 nm feature size thermochemical nanolithography," *Nano Letters*, **7**(4), pp. 1064–1069.

[27] Park, K., J. Lee, R. Bhargava, and W. P. King (2008) "Routine femtogram-level chemical analyses using vibrational spectroscopy and self-cleaning scanning probe microscopy tips," *Analytical Chemistry*, **80**(9), pp. 3221–3228.

[28] Lee, J., A. Liao, E. Pop, and W. P. King (2009) "Electrical and Thermal Coupling to a Single-Wall Carbon Nanotube Device Using an Electrothermal Nanoprobe," *Nano Letters*, **9**(0), p. 1356.

[29] Lee, J., T. L. Wright, M. R. Abel, E. O. Sunden, A. Marchenkov, S. Graham, and W. P. King (2007) "Thermal conduction from microcantilever heaters in partial vacuum," *Journal of Applied Physics*, **101**(1), p. 6.

[30] Park, K., A. Marchenkov, Z. M. M. Zhang, and W. P. King (2007) "Low temperature characterization of heated microcantilevers," *Journal of Applied Physics*, **101**(9), p. 9.

[31] Lee, J. and W. P. King (2008) "Liquid Operation of Silicon Microcantilever Heaters," *IEEE Sensors Journal*, **8**(11-12), pp. 1805–1806, lee, Jungchul King, William P.

[32] Dames, C. and G. Chen (2005) "1 omega, 2 omega, and 3 omega methods for measurements of thermal properties," *Review of Scientific Instruments*, **76**(12).

[33] Park, K., J. Lee, Z. M. M. Zhang, and W. P. King (2007) "Frequency-dependent electrical and thermal response of heated atomic force microscope cantilevers," *Journal of Microelectromechanical Systems*, **16**(2), pp. 213–222.

[34] De Marzi, G., D. Lacopino, A. J. Quinn, and G. Redmond (2004) "Probing intrinsic transport properties of single metal nanowires: Direct-write contact formation using a focused ion beam," *Journal of Applied Physics*, **96**(6), pp. 3458–3462.

[35] Zhang, Q. G., B. Y. Cao, X. Zhang, M. Fujii, and K. Takahashi (2006) "Size effects on the thermal conductivity of polycrystalline platinum nanofilms," *Journal of Physics-Condensed Matter*, **18**(34), pp. 7937–7950.